Load Transfer Behavior of Full-Scale Instrumented Helical Piles

Kristen M. Tappenden
Thurber Engineering Ltd, Edmonton, Alberta, Canada
Ehsan Abazari
Department of Civil and Environmental Engineering – University of Alberta, Edmonton, Alberta, Canada
David C. Sego
Department of Civil and Environmental Engineering – University of Alberta, Edmonton, Alberta, Canada

ABSTRACT
A field load testing program was undertaken to study the load transfer behavior of full-scale, instrumented helical piles installed in clay and sand soils. Five piles were fabricated of 219-mm-diameter hollow circular steel shafts each affixed with three 356-mm-diameter steel helices, spaced at 1.5 times the helix diameter. Each helical pile was instrumented with strain gauges at five locations along the inside wall of the pile shaft. Four of the five instrumented piles were installed to 5.0 m, with two tested in uplift and two in compression; the fifth pile was installed to 3.0 m and tested in uplift. Strain gauge readings collected during the axial load tests were used to characterize the stress transfer along the length of the test piles to the surrounding soil. The resulting load distribution curves for the five test piles are presented in this paper. The load distribution curves and ultimate axial capacities are compared to theoretical values calculated by the Cylindrical Shear and Individual Plate Bearing models, and discrepancies between the models and the measured distributions are discussed.

RÉSUMÉ
Un programme d'essais de charge sur le terrain a été entrepris pour étudier le comportement de transfert de charge des pieux hélicoïdaux instrumentés à pleine échelle installés dans les sols argileux et sableux. Cinq piles ont été fabriquées à partir d'arbres creux circulaires en acier de 219 mm de diamètre fixés chacun à l'aide de trois hélices en acier de 356 mm de diamètre, espacées de 1,5 fois le diamètre de l'hélice. Chaque pile hélicoïdale a été instrumentée avec des jauges de contrainte à cinq endroits le long de la paroi intérieure de l'arbre de pieux. Quatre des cinq piles instrumentées ont été installées à 5,0 m, deux d'entre elles étant soumises à un soulèvement et deux à la compression; la cinquième pile a été installée à 3,0 m et testée en soulèvement. Les lectures des jauges de contrainte recueillies au cours des essais de charge axiale ont été utilisées pour caractériser le transfert des contraintes le long des pieux d'essai vers le sol environnant. Les courbes de distribution de charge résultantes pour les cinq piles d'essai sont présentées dans cet article. Les courbes de distribution de charge et les capacités axiales ultimes sont comparées aux valeurs théoriques calculées par les modèles Cylindrical Shear et Individual Plate Bearing, et les discordances entre les modèles et les distributions mesurées sont discutées.

1 INTRODUCTION

Helical piles, also known as screw anchors or screw piles, are deep foundation elements comprised of one or more circular helical plates affixed to a central shaft of smaller diameter. The shaft of the helical pile is frequently manufactured from standard sizes of hollow steel pipe, typically ranging from about 114 mm to 320 mm in diameter; helical piles fabricated from hollow circular shafts are typically fitted with steel helical plates having a diameter of 2 to 3 times the shaft diameter.

Helical piles are embedded into the ground by applying a turning moment to the head of the pile shaft, which causes the helix or helices to penetrate the soil in a screwing motion, without producing any spoil. Installation of helical piles can be accomplished using relatively light weight equipment, such as a torque head affixed to the arm of a backhoe or to a trailer-mounted hydraulic boom.

This paper presents the results of a field research program to study the axial load distribution for full-scale helical piles loaded in compression and uplift. Commercially manufactured circular-shaft helical piles were instrumented with strain gauges at incremental locations along the pile shaft, and embedded into glaciolacustrine clay and aeolian sand soils near Edmonton, Alberta. The stress distributions along the length of the test piles during axial loading, as derived from the strain gauge readings, are presented in this paper. The transfer of axial load from the helical pile to the surrounding soil is discussed in the context of existing helical pile failure models, which were primarily developed based on laboratory-scale tests (e.g. Narasimha Rao et al. 1993, Narasimha Rao and Prasad 1991). Discrepancies between the measured and expected load transfer distributions are discussed.

2 METHODOLOGY

2.1 Fabrication and Instrumentation of Test Piles

For this research program, five triple-helix steel helical piles were fabricated by welding three 356 mm diameter helices to 219 mm diameter hollow circular shafts. The three helices were vertically spaced along the pile shafts at a distance equal to 1.5 times the helix diameter (533 mm). This normalized spacing of the helices divided by their average diameter, is termed the inter-helix spacing ratio.

The pitch of the helices was 76 mm. Four of the test piles were fabricated to 'long' lengths of 5.18 m, while one test pile was fabricated to a 'short' length of 3.05 m. The dimensions of the test piles, designated C1 to C2 and T1 to T3, are summarized in Table 1 below.

Each test pile was instrumented with strain gauges installed at five levels along the inside wall of the pile shaft. At each level, three axial strain gauges were installed 120 degrees apart around the inside circumference of the pile shaft, so as to negate the effects of any bending or eccentric loading of the shaft. Strain rosettes were used in this research; each rosette had three gauges whose axes were 45 degrees apart (Zhang 1999). The strain gauges were protected by a silicone shell and fibreglass insulation to avoid damage by extreme heating during assembly of the test piles (which were welded together in sections following placement of the strain gauges), and to prevent moisture damage during field testing. An electronic data logger was used to monitor the real-time results and store the data collected (Zhang 1999). Additional details regarding the method for assembling the test piles and affixing the strain gauges are presented in Zhang (1999).

3 SURFICIAL GEOLOGY OF LOAD TEST SITES

The field program included five static axial pile load tests performed at two sites representing cohesive and cohesionless soils, respectively. The surficial soils at the chosen test sites comprised glaciolacustrine clay at the University of Alberta Experimental Farm in Edmonton, Alberta, and aeolian sand near the town of Bruderheim, 60 km northeast of Edmonton. A geotechical field investigation was conducted at each of the test sites, which included auger drilling, standard penetration testing and cone penetration testing for in-situ characterization of the surficial soils. Unconfined compressive strength tests and shear vane tests were also conducted on samples of the cohesive soils collected at the Edmonton site.

At the University Farm test site in Edmonton, the glaciolacustrine sediments consist of varved silts and clays, typically becoming more silty and sandy with depth (Bayrock and Hughes 1962). Within the zone of influence of the test piles, the stratigraphy generally consisted of high plastic silty clay, with liquid limits of approximately 60 to 70 percent, and corresponding plasticity indices of 30 to 40 (Bhanot 1968). The groundwater level was located at a depth of approximately 3 m. CPT and SPT profiles were obtained during the field investigation at the Edmonton site. The undrained shear strength of the stiff silty clay was estimated to be approximately 50 kPa from 0 to 1.5 m, and 80 kPa from 1.5 m to the base of the test piles, based on unconfined compressive strength and shear vane tests, and correlations to Standard Penetration and Cone Penetration Tests, as shown in Figure 1 (correlations from Lunne and Kleven 1981, Terzaghi and Peck 1967).

The Bruderheim test site is located in central Alberta, approximately 60 km northeast of the city of Edmonton, and approximately 7.5 km north of the Bruderheim town centre. The surficial stratigraphy of the site consists of fine-to-medium grained silty sand formed from dried sediments of proglacial Lake Edmonton that were transported by wind after the drainage of the lake and deposited as sand dunes with minor loess (Zhang 1999). The stratigraphy within the depth of the test pile installations consisted of loose to compact silty sand. The groundwater level was located at a depth of approximately 4.5 m. CPT and SPT profiles were obtained during the field investigation at the Bruderheim site. The estimated friction angle of the sand was approximately 37 degrees in the upper dessicated crust 3 m, and 28 degrees below, based on published correlations (from Bowles 1988, De Mello 1971) to the measured Standard Penetration Test (SPT) N values, as shown in Figure 2. Figure 2 also displays the friction angle estimated by Robertson and Campanella's (1983) correlation to the Cone Penetration Test (CPT) results. However, based on local experience, the friction angles estimated by the CPT correlation were not considered to be representative of the in-situ soil conditions, and therefore were not used in the estimation of the representative soil strength parameters.

Table 1. Summary of Test Pile Dimensions

Test Pile	Pile Length (m)	Diameter of Shaft, d (mm)	Diameter of Helices, D (mm)	Depth to H_1 (m)	Depth to H_2 (m)	Depth to H_3 (m)	Inter-helix Spacing Ratio (S/D)
C1	5.0	219	356	3.72	4.25	4.79	1.5
T1	5.0	219	356	3.72	4.25	4.79	1.5
T2	3.0	219	356	1.67	2.20	2.74	1.5
C2	5.0	219	356	3.72	4.25	4.79	1.5
T3	5.0	219	356	3.72	4.25	4.79	1.5

Notes: S = vertical spacing between adjacent helices along the pile shaft

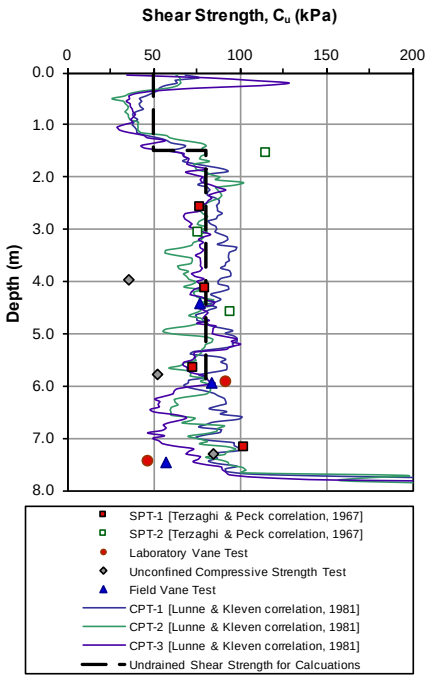

Figure 1. Edmonton (clay) site; profile of undrained shear strength from correlations to in-situ and laboratory tests.

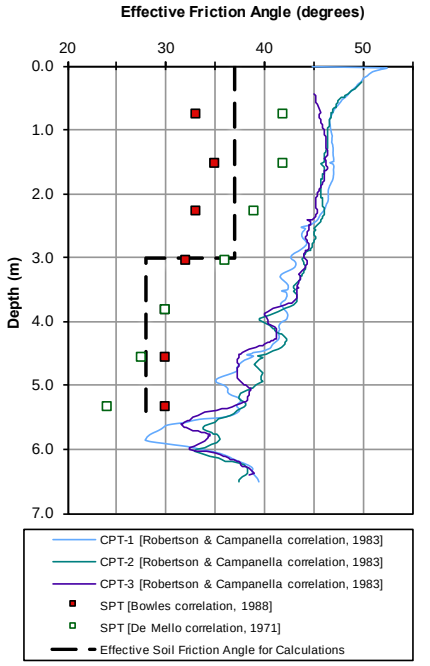

Figure 2. Bruderheim (sand) site; profile of soil friction angle from correlations to in-situ tests.

4 PILE LOAD TESTING PROGRAM

A total of five instrumented helical piles were installed and tested at the subject sites. At the Edmonton (clay) site, one long (5.0 m) pile was tested in compression, and one long and one short (3.0 m) pile were tested in uplift. At the Bruderheim (sand) site, one long pile was tested in compression, and one long pile was tested in uplift. Each of the test piles were loaded in either compression or tension in accordance with the ASTM "quick test" procedures for static pile load testing (ASTM D 1143-81 and D 3689-90). Each pile was loaded to failure in increments of 10 to 15 percent of the proposed design load. Each loading increment was held until the rate of deflection decreased below 0.25 mm per hour. Load increments were added until the onset of plunging failure (continuous jacking required to maintain the applied load), or until a vertical displacement equal to 10 percent of the helix diameter was achieved. This maximum load was held for 5 minutes and then removed. Throughout the duration of load testing, strain gauge measurements along the instrumented pile shaft were electronically collected and stored in the data logger (Zhang 1999).

Reactions for the axial compression and tension tests were developed from two triple-helix screw anchors installed to a depth of 5.0 m at a distance of at least 2.75 m on either side of the test pile. Details of the field load test apparatus and the test program are presented in Zhang (1999).

5 LOAD TEST RESULTS

5.1 Measured Ultimate Pile Capacities

For the purposes of the field research program, the ultimate axial capacity of the test piles was defined as the lesser of the applied load at the onset of plunging failure (that is, continuous jacking required to maintain the test load), or the applied load required to induce a displacement equal to 10 percent of the helix diameter (35 mm). It is generally acknowledged that a vertical displacement of about 10 percent of the pile diameter is adequate to mobilize the ultimate pile shaft friction and majority of the tip resistance for most piles (Kulhawy 1984). The ultimate axial pile capacities from the load tests are summarized in Table 2 below. Table 2 also includes the pile installation depths and the maximum torque readings recorded at the depth of the pile installations. The load-settlement curves for each of the test piles are presented in Zhang (1999).

5.2 Measured Load Distribution Curves

Figures 3 to 7 present the load distribution curves for the instrumented test piles, derived from the strain gauge measurements recorded at five levels along the helical pile shafts, at six increments of applied loading, up to the ultimate pile capacity in tension or compression. The shape of the recorded load distribution curves characterizes the mechanism of load transfer along the length of the test piles to the surrounding soils. The right-most load distribution curve in Figures 3 to 7 represents the distribution of applied load along the test pile at the ultimate axial capacity ("failure"). The change in measured load between two strain gauges represents the portion of the applied load that is transferred to the soil by frictional and/or bearing mechanisms acting along the corresponding length of the test pile.

Table 2. Test Pile Installation Locations, Depths and Ultimate Axial Resistance by Static Load Test

Test Pile	Location	Soil Type	Installation Depth (m)	Loading Direction	Applied Load at Failure (kN)	Maximum Installation Torque (kNm)
C1	Edmonton	Stiff silty clay	5.0	Compression	190[a]	20.3
T1	Edmonton	Stiff silty clay	5.0	Uplift	215[b]	22.0
T2	Edmonton	Stiff silty clay	3.0	Uplift	145[b]	20.3
C2	Bruderheim	Loose to compact sand	5.0	Compression	480[b]	44.7
T3	Bruderheim	Loose to compact sand	5.0	Uplift	365[a]	50.8

Notes: a) axial load at vertical displacement equal to 10% of the helix diameter (35 mm)
b) axial load at onset of plunging failure (continuous jacking required to maintain applied load)

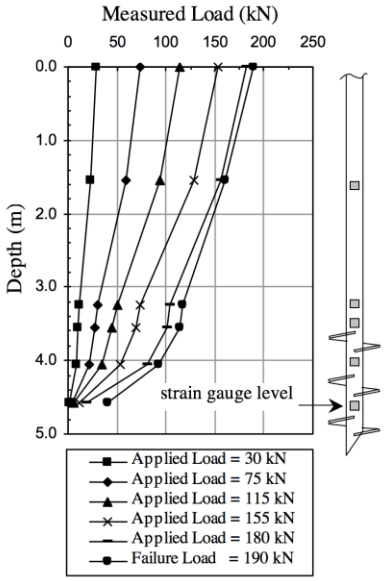

Figure 3. Measured Load Distribution Curves: Pile C1, Edmonton (Clay) Site

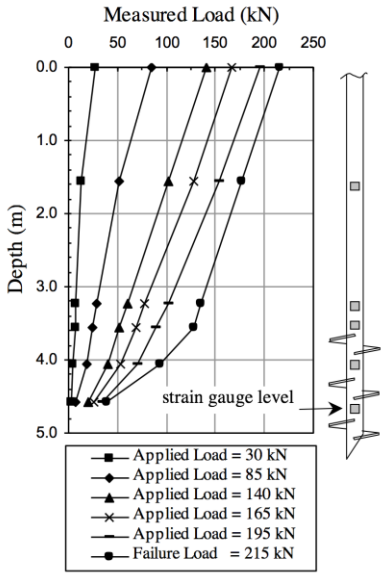

Figure 4. Measured Load Distribution Curves: Pile T1, Edmonton (Clay) Site

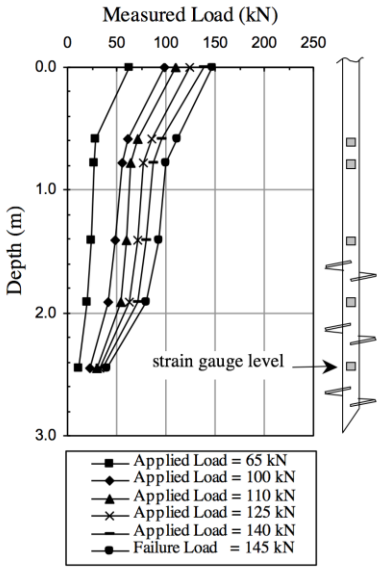

Figure 5. Measured Load Distribution Curves: Pile T2, Edmonton (Clay) Site

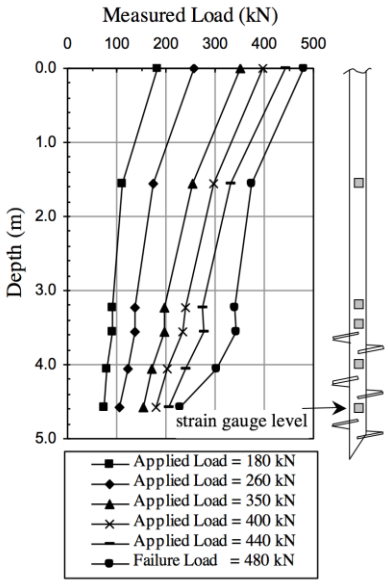

Figure 6. Measured Load Distribution Curves: Pile C2, Bruderheim (Sand) Site

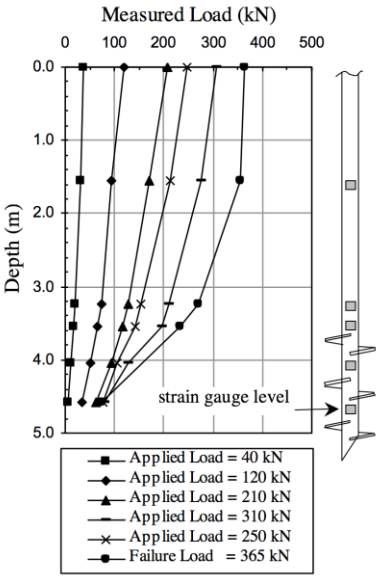

Figure 7. Measured Load Distribution Curves: Pile T3, Bruderheim (Sand) Site

6 DISCUSSION OF RESULTS

6.1 Helical Pile Failure Models

Two primary failure models have been proposed in the literature for describing the behavior of helical piles under axial loading—these are the individual plate bearing model (Adams and Klym 1972, Narasimha Rao et al. 1993) and the cylindrical shear model (Mitsch and Clemence 1985, Mooney et al. 1985, Narasimha Rao and Prasad 1991).

The individual plate-bearing model assumes the helical pile behaves as a series of independent plates, whereby each helix acts independently of the others in bearing or uplift. The pile's axial capacity is therefore taken as the sum of the bearing capacities of the individual helices in compression or tension (Figure 8a and b).

The cylindrical shear model assumes the formation of a cylindrical failure surface, circumscribed between the uppermost and lowermost helices of the pile, during axial loading. The axial capacity of the helical pile is presumed to consist of shear resistance along this cylindrical surface and bearing resistance above the top helix (in tension) or below the bottom helix (in compression) (Figure 8c and d).

Skin friction acting along the section of the pile shaft between the uppermost helix and the ground surface may also be considered to contribute to the axial capacity, in both the cylindrical shear and the individual plate bearing models. This shaft friction component may be of considerable importance for deeply installed piles. It is generally concluded, however, that under tensile loading, skin friction should be neglected along the portion of the pile shaft contained within the zone of bearing failure above the uppermost helix. This bearing zone may be considered to extend a distance approximately equal to the diameter of the uppermost helix for deeply embedded piles (Zhang 1999). For shallow helical piles in uplift, the zone of bearing failure above the top helix extends to the ground surface, and the skin friction component along the entire shaft length should therefore be neglected (Mitsch and Clemence 1985).

The choice of the most representative failure model to describe the behavior of helical piles under axial loading is considered to be a function of the pile geometry. It is well established that the failure zone at the tip of a pile extends over a depth of almost twice the pile diameter (Zeevaert 1983). For this reason, the assumption that the helical plates behave independently of one another (as per the individual plate bearing model) is only considered valid for multi-helix piles with inter-helix spacing ratios greater than 2.0 (Narasimha Rao et al. 1993). For multi-helix piles with spacing ratios of less than 2.0, as used in the current study, interaction between the closely spaced helical plates under axial loading is generally considered to create a failure surface better represented by the cylindrical shear model. The cylindrical shear model has been primarily established on the basis of laboratory uplift tests performed on model helical piles installed in sand, silt, and clay (Mitsch and Clemence 1985; Mooney et al. 1985; Narasimha Rao et al. 1993; Narasimha Rao et al. 1989), and has also been applied to laboratory compression tests performed on model helical piles installed in clay (Narasimha Rao et al. 1991).

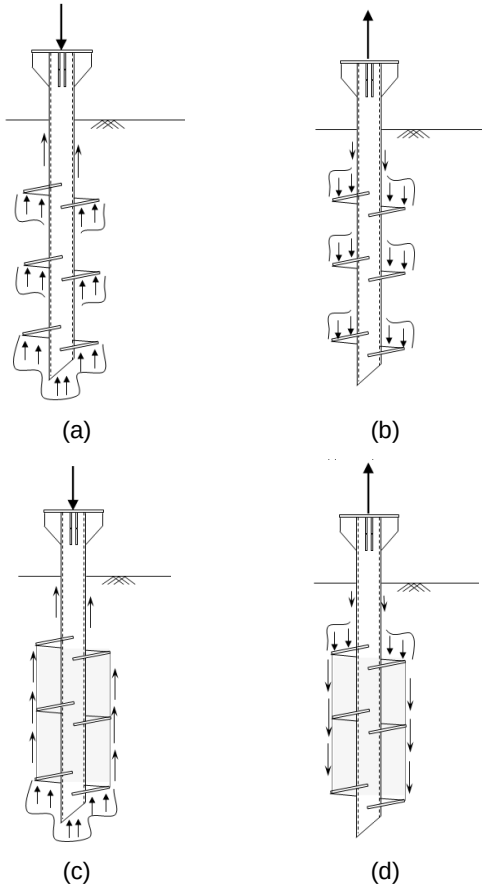

Figure 8. Helical Pile Failure Models (not to scale):
(a) Individual Plate Bearing Model under compression, and (b) uplift (after Mooney et al. 1985);
(c) Cylindrical Shear Model under compression, and
(d) uplift (after Narasimha Rao et al. 1991).

6.2 Estimated Ultimate Pile Capacities and Load Distributions

For comparison with the measured load distributions, the ultimate theoretical axial load distributions were calculated for the test piles using both the cylindrical shear model and the individual plate bearing model. The components of shaft friction, cylindrical friction and plate bearing comprising the ultimate helical pile capacities in tension and compression were calculated using the published formulas summarized in Tappenden (2007). For the bearing capacity of helical plates in cohesive soil (Equation 1), a bearing capacity factor of N_c equal to 9 was used for the 'long' piles in compression and uplift (CFEM 2006). For the 'short' pile in uplift, the N_c factor was calculated as per Equation 2 below, from Meyerhof (1976). For the bearing capacity of helical plates in cohesionless soils (Equation 3), an N_q factor of 20 was used in bearing and in uplift, for helices installed in the loose, silty sand at the Bruderheim site with an approximate friction angle of 28 degrees (refer to Figure 9 from Das (1990)). This is similar to the value recommended by Vesic (1963) for N_q (bearing) in cohesionless soils.

$$Q_u = (N_c C_u)\frac{\pi(D^2 - d^2)}{4} \quad [1]$$

$$N_c = 1.2\left(\frac{H_1}{D_1}\right) \leq 9.0 \quad [2]$$

$$Q_b = N_q \gamma' H \frac{\pi(D^2 - d^2)}{4} \quad [3]$$

H = depth of helix below ground surface (m)
D = diameter of helix (m)
d = diameter of pile shaft (m)
N_c = bearing capacity factor, cohesive soil
C_u = undrained shear strength of cohesive soil (kPa)
N_q = bearing capacity factor, cohesionless soil (Fig. 9)
γ' = effective soil unit weight (kN/m^3)
γ = total soil unit weight (kN/m^3)

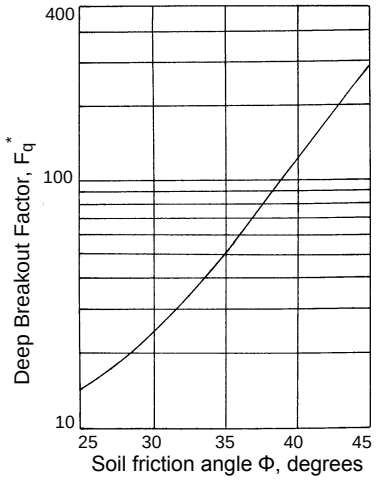

Figure 9: Variation of breakout factor, deep condition (after Das, 1990)

For the components of shaft friction and cylindrical shear (cylindrical shear model), the formulae presented in Tappenden (2007) were used. In clay, the values of the adhesion factor given in the Canadian Foundation Engineering Manual CFEM 2006) for grouted anchors in cohesive soils were used for calculating the shaft friction and the cylindrical shear friction. In sand, δ, the angle of friction between the pile shaft and soil was taken as 60% of the effective soil friction angle (Kulhawy 1984).

The experimentally-derived values for K, proposed by Mitsch and Clemence (1985) for helical piles loaded in uplift in sand, were used in the current study for estimating both the compressive and tensile resistance of the helical piles at the Bruderheim site. Mitsch and Clemence (1985) proposed values for the parameter K on the basis of full-scale field and laboratory uplift tests on multi-helix piles in sand, as shown in Table 3. The K values suggested by Mitsch and Clemence (1985) are approximately 40 percent less than the K values proposed by Meyerhof and Adams (1968) for the uplift capacity of buried foundations. Mitsch and Clemence (1985) attributed the lower coefficients for helical piles to the disturbance created by the churning action of the helices during installation; Meyerhof and Adams' (1968) values, however, were based on essentially undisturbed soil.

Except for relatively slender piles that may contract radially under tensile load, current opinion would state that there is no systematic difference in the value of skin friction that may be mobilized by a pile loaded either in tension or compression (Fleming et al. 1992). As such the experimentally-derived K values, proposed by Mitsch and Clemence (1985) for use with helical piles under uplift in sand, were used in the current study for estimating both the compressive and tensile resistance of the helical piles in sand. It may be noted that Mitsch and Clemence's (1985) K values for helical piles in loose to compact sand ($\phi \leq 35°$) are in general agreement with the range of K values suggested by Fleming et al. (1992) for driven piles in cohesionless soils.

$$Q_{cyl} = \pi \cdot d \cdot C_u \cdot \alpha \cdot (H_n - H_1) \quad [4]$$

$$Q_{cyl} = \pi \cdot D \cdot \left(\frac{1}{2}\gamma' K \tan\phi\right) \cdot \left(H_n^2 - H_1^2\right) \quad [5]$$

K = lateral earth pressure coefficient for helical piles (Table 3)
α = adhesion factor for anchors in cohesive soil (CFEM 2006)
H_n = depth of lowermost helix below ground (m)
H_1 = depth of uppermost helix below ground (m)

Table 3. Recommended K values for screw piles (after Mitsch and Clemence 1985)

Effective soil friction angle, ϕ	Lateral earth pressure coefficient, K
25°	0.70
30°	0.90
35°	1.50
40°	2.35
45°	3.20

Soil strength parameters estimated from the field and laboratory investigations, as previously depicted in Figures 1 and 2, were used in the calculations. Table 4 summarizes the ultimate axial capacities calculated for each of the test piles using the individual plate bearing and cylindrical shear models.

The cumulative components of the theoretical helical pile capacities were then plotted to correspond with the depth of the strain gauge installations. Figures 10 to 14 show the load distributions calculated using the cylindrical shear model and the individual plate bearing model, compared to the measured ultimate load distributions for each of the five test piles.

Table 4. Comparison of Measured and Calculated Ultimate Pile Resistances

Test Pile	Applied Load at Failure (kN)	Calculated Axial Resistance (kN)	
		Cylindrical Shear Model	Individual Plate Bearing Model
C1	190[a]	207	248
T1	215[b]	227	221
T2	145[b]	157	149
C2	480[b]	292	450
T3	365[a]	199	378

Notes: a) axial load at 35 mm displacement
b) axial load at onset of plunging failure

6.3 Comparison of Measured and Theoretical Results

For pile C1 tested in compression at the Edmonton (clay) site, the cylindrical shear model provided a good estimate of the ultimate capacity (within approximately 9 percent, Table 4). The individual plate bearing model significantly over-estimated the ultimate capacity of pile C1 in compression by approximately 30 percent (Table 4). Due to the close spacing of the helical plates for the test piles used in this study (S/D = 1.5), it is not surprising that the measured load transfer to the soil was less than the summation of the calculated individual bearing capacities of the helices. Notwithstanding, the load distribution curve calculated using the individual plate bearing model for pile C1 relatively well-represented the *shape* of the measured curve (Figure 10). The discrepancy between the measured curve and the individual plate bearing curve was mainly due to the lesser contribution of the bottom helix in bearing (as captured by the lowermost strain gauge). It is possible that the soil plug in the pile shaft was not fully formed at the installed depth of 5.0 m, or that the ultimate bearing capacity was not fully developed below the lowermost helix when the test was terminated at a vertical displacement 35 mm.

For the two piles tested in tension at the Edmonton (clay) site, both the cylindrical shear and the individual plate bearing models provided estimates of the ultimate tensile capacities that were within approximately 8 percent of the measured failure loads. Despite notable discrepancies between the measured and calculated load distribution curves, the individual plate bearing model provided slightly better approximations of the measured load distributions in uplift for both the 'long' and 'short' piles (Figures 11 and 12).

At the Bruderheim (sand) site, the ultimate capacities of piles C2 in compression, and T3 in tension, estimated using the individual plate bearing model were within approximately 6 percent of the measured ultimate capacities (Table 4). The cylindrical shear model, on the other hand, substantially underestimated the ultimate capacities in compression and tension by 40 and 45 percent, respectively. The shape of the measured load distribution curves were also better represented by the individual plate bearing model (Figures 13 and 14), though there are evident discrepancies.

In summary, at the Edmonton (clay) site, the behavior of the helical piles in cohesive soils was better represented by the cylindrical shear model. However, at the Bruderheim (sand) site, the behavior of the helical piles in cohesionless soils was more accurately captured using the individual plate bearing model, in spite of the closely-spaced helices.

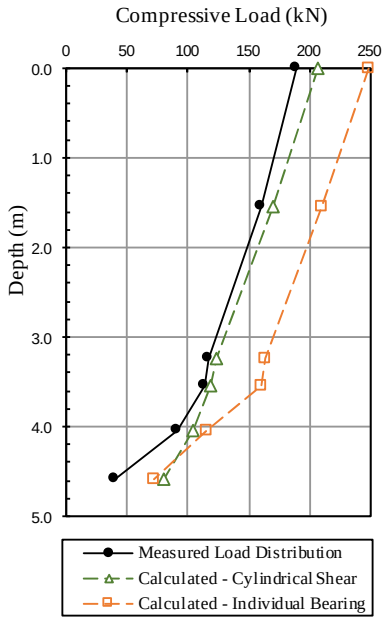

Figure 10. Measured Load Distribution at Failure compared to Calculated Values, Pile C1, Edmonton (Clay) Site

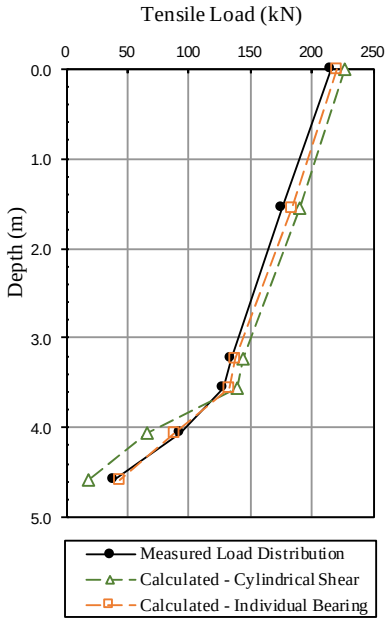

Figure 11. Measured Load Distribution at Failure compared to Calculated Values, Pile T1, Edmonton (Clay) Site

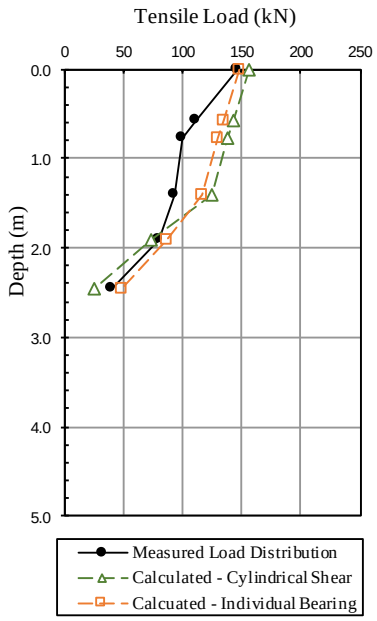

Figure 12. Measured Load Distribution at Failure compared to Calculated Values, Pile T2, Edmonton (Clay) Site

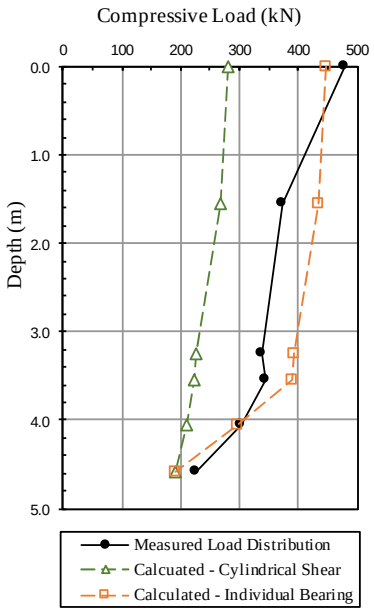

Figure 13. Measured Load Distribution at Failure compared to Calculated Values, Pile C2, Bruderheim (Sand) Site

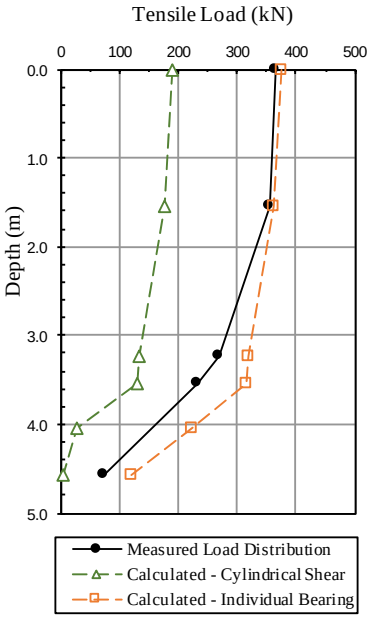

Figure 14. Measured Load Distribution at Failure compared to Calculated Values, Pile T3, Bruderheim (Sand) Site

7 CONCLUSIONS

A load testing program of full-scale, instrumented helical piles was undertaken to investigate the load transfer mechanism between multi-helix piles and the surrounding soil during axial loading. Five circular shaft, triple-helix piles were instrumented with strain gauges and installed at two separate test sites comprising glaciolacustrine clay and aeolian sand soils. At each test site, the helical piles were loaded to failure in compression and tension in accordance with the ASTM “quick test” procedures for static pile load testing (ASTM D 1143-81 and D 3689-90). The resulting load distribution curves determined at various stages of applied compressive or tensile load were presented for each of the five test piles.

The measured load distributions at the ultimate compressive or tensile capacities were compared to the theoretical ultimate load distributions calculated using the cylindrical shear and individual plate bearing models. The pile capacities calculated using the individual plate bearing model are particularly sensitive to the value chosen for N_c (in cohesive soils) and N_q (in cohesionless soils). At the Bruderheim (sand) site, a conservative N_q value of 20 was used in both compression and uplift, based on Das (1990) and Vesic (1963), for the inferred soil friction angle of 28 degrees.

With the exception of pile C1, the individual plate bearing model provided very good estimates (within approximately 6 percent) of the ultimate axial helical pile capacities (Table 4), and reasonably captured the shape of the measured ultimate load distributions along the piles at failure (Figures 10 to 14). Perhaps due to the close spacing between the helical plates (S/D = 1.5), at the Edmonton (clay) site, the behavior of the helical piles in cohesive soils was better represented by the cylindrical shear model. However, at the Bruderheim (sand) site, the behavior of the helical piles in cohesionless soils was more accurately captured using the individual plate bearing model.

ACKNOWLEDGEMENTS

The authors wish to acknowledge Diane Zhang and Gerry Cyre for their work in instrumenting the test anchors, and conducting and documenting the pile load tests described in this paper. ConeTec Inc. and Almita Manufacturing Ltd. are thanked for their partnership and financial support of the research work presented herein.

REFERENCES

Adams, J.I. and Klym, T.W. (1972). The uplift capacity of shallow foundations. Ontario Hydro Research Quarterly, 19:1-13.

Bayrock, L.A. and Hughes, G.M. (1962). Surficial geology of the Edmonton district, Alberta. Research Council of Alberta, Preliminary Report 62-6, 40 p.

Bhanot, K.L. (1968). Behavior of scaled and full-length cast-in-place concrete piles. *PhD Thesis,* Dept. of Civil Engineering, University of Alberta, Edmonton, Alberta, 336 p.

Bowles, J.E. (1988). Foundation analysis and design. 4th ed., McGraw-Hill, New York, 1004 p.

CFEM. (2006). Canadian foundation engineering manual, 4th ed., Canadian Geotechnical Society, Richmond, British Columbia, Canada.

Das, B.M. (1990). Earth anchors. Elsevier, New York, 241 p.

De Mello, V.F.B. (1971). “The standard penetration test.” *Proceedings of the Fourth Panamerican Conference on Soil Mechanics and Foundation Engineering*, ASCE, Vol. 1: 1-86.

Fleming, W.G.K, Weltman, A.J., Randolph, M.F. and Elson, W.K. (1992). Piling engineering, John Wiley & Sons, Inc., New York, 2nd Edition, 390 p.

Hoyt, R.M. and Clemence, S.P. (1989). “Uplift capacity of helical anchors in soil.” *Proceedings of the 12th International Conference on Soil Mechanics and Foundation Engineering.* Rio de Janeiro, Brazil, 2: 1019-1022.

Kulhawy, F.H. (1984). “Limiting tip and side resistance: fact or fallacy?” *Analysis and Design of Pile Foundations,* ASCE, New York: 80-98.

Lunne, T. and Kleven, A. (1981). “Role of CPT in North Sea foundation engineering.” *Cone Penetration Testing and Experience: Proceedings of a Session Sponsored by the Geotechnical Engineering Division at the ASCE National Convention,* St. Louis, Missouri: 76-107.

Mitsch, M.P. and Clemence, S.P. (1985). “The uplift capacity of helix anchors in sand.” *Uplift Behaviour of Anchor Foundations in Soil*, ASCE, New York: 27-47.

Meyerhof, G.G. (1976). “Bearing capacity and settlement of pile foundations.” *Journal of Geotechnical Engineering*, ASCE, 102(GT3): 197-224.

Meyerhof, G.G., and Adams, J.I. (1968). “The ultimate uplift capacity of foundations.” *Canadian Geotechnical Journal,* 5(4): 224-244.

Mooney, J.S., Adamczak, S. Jr. and Clemence, S.P. (1985). “Uplift capacity of helical anchors in clay and silt.” *Uplift Behaviour of Anchor Foundations in Soil*, ASCE, New York: 49-72.

Narasimha Rao, S., Prasad, Y.V.S.N. and Veeresh, C. (1993). “Behaviour of embedded model screw anchors in soft clays.” *Geotechnique* 43(4): 605-614.

Narasimha Rao, S., Prasad, Y.V.S.N. and Shetty, M.D. (1991). “The behaviour of model screw piles in cohesive soils.” *Japanese Society of Soil Mechanics and Foundation Engineering* 31(2): 35-50.

Narasimha Rao, S., Prasad, Y.V.S.N., Shetty, M.D. and Joshi, V.V. (1989). “Uplift capacity of screw pile anchors.” *Geotechnical Engineering* 20: 139-159.

Robertson, P.K. and Campanella, R.G. (1983). “Interpretation of cone penetration tests: sands.” *Canadian Geotechnical Journal* 20(4): 719-733.

Tappenden, K.M. and Sego, D.C. (2007). “Predicting the axial capacity of screw piles installed in Canadian soils.” *Proc. 60th Canadian Geotechnical Conference,* Ottawa, p. 1608-1615.

Terzaghi, K. and Peck, R.B. (1967). Soil mechanics in engineering practice. John Wiley and Sons, New York, 729 p.

Vesic, A. 1963. Bearing capacity of deep foundations in sand, Highway Research Record, 39,National Academy of Sciences, National Research Council, p.112-153.

Zeevaert, L. (1983). Foundation engineering for difficult subsoil conditions. Van Nostrand Reinhold, New York, 2nd Edition, 652 p.

Zhang, D. (1999). Predicting capacity of helical screw piles in Alberta soils. *MSc Thesis*, Dept. of Civil and Environmental Engineering, University of Alberta, Edmonton, Alberta, 304 p.